Chinese Chemical Letters 35 (2024) 109492

Contents lists available at ScienceDirect

Chinese Chemical Letters

journal homepage: www.elsevier.com/locate/cclet

Catalytic applications of amorphous alloys in wastewater treatment: A review on mechanisms, recent trends, challenges and future directions

Yulong Liu, Haoran Lu, Tong Yang, Peng Cheng, Xu Han, Wenyan Liang*

Engineering Research Center for Water Pollution Source Control & Eco-remediation, Beijing Key Lab for Source Control Technology of Water Pollution, College of Environmental Science and Engineering, Beijing Forestry University, Beijing 100083, China

ARTICLE INFO

Article history:
Received 24 September 2023
Revised 9 December 2023
Accepted 2 January 2024
Available online 5 January 2024

Keywords:
Amorphous alloys
Wastewater treatment
Advanced oxidation processes
Catalyst
Catalytic mechanism

ABSTRACT

Amorphous alloys, with unique atomic structures and metastable nature, are treated as superior candidates for environmental wastewater remediation due to their superior catalytic capabilities. Given the strong demand for environmental protection, the field of amorphous alloys in wastewater treatment has great development prospects, and numerous research results have been published in recent years. As a promising catalyst, it was demonstrated that amorphous alloys could exhibit many excellent properties in wastewater treatment, such as high catalytic efficiency, easily adjustable parameters and reliable sustainability. This paper aims to summarize recent research trends regarding amorphous alloys in the field of catalysis, focusing on the preparation methods, physical performance, catalytic mechanisms and environmental application. Meanwhile, this review also investigates the challenges encountered and future perspectives of amorphous alloys, offering new research opportunities to enlarge their applicability spectra.

© 2024 Published by Elsevier B.V. on behalf of Chinese Chemical Society and Institute of Materia Medica, Chinese Academy of Medical Sciences.

1. Introduction

Water pollution has become a serious environmental problem along with the rapid development of modern industries. With the improvement of environmental awareness, wastewater treatment techniques have been vigorously developed [1]. Advanced oxidation processes (AOPs), including photocatalysis [2], ozone [3], Fenton and Fenton-like oxidation [4,5], and electrochemical catalysis [6], have been extensively studied as promising techniques due to their superior degradation and mineralization efficiency on pollutants in wastewater. Highly reactive and transitory species are the primary oxidants employed in AOPs and can be activated by catalysts [7]. For instance, the reported single-atom catalysts and high-valent metal species in recent years have been applied in the field of environmental remediation because of their good selectivity [8–10]. However, zero-valent metal single atoms are extremely unstable, requiring solid host materials to bear ligating atoms to form chemical bonds with metal single atoms [11]. While amorphous alloys can overcome such problems, because the zero-valent metal atoms are embedded in the alloy, such as Fe^0 in Fe-based amorphous alloys.

Amorphous alloys, also called metallic glasses, with short-range ordered and long-range disordered atomic structures, have recently attracted increasing attention as advanced functional materials [12]. As shown in Table 1 [13–21], many unique properties, such as high strength and elasticity, superior anti-corrosion behavior, excellent wear resistance and attractive soft/hard magnetic performance, compared to crystalline counterparts or pure metals, have been discovered for amorphous alloys. Moreover, these investigations could provide new insights into commercial applications and fundamental studies. The first known successful preparation of amorphous alloy was gold-silicon alloy, prepared in 1960, which was observed with highly disordered arrangements of the atoms, similar to that of the liquid state [22]. After that, amorphous alloys with the unique atomic packing structure as metastable materials have been carried out by plenty of researchers and widely used in space exploration [23,24], resonators, electrical components and biomedical equipment [25–27].

Recent reports demonstrate that amorphous alloys have both favorable catalytic capacity and unique selectivity properties and have become a new promising catalyst for wastewater treatment [28]. Many research outcomes have exhibited the fast-catalytic efficiency, excellent sustainability, and high stability of amorphous alloys [29]. For instance, concerning water treatment, the $Fe_{76}B_{12}Si_9Y_3$ powder showed 1000 times higher reactivity than crystalline Fe powder in treating methyl orange [30]. Moreover, the Fe-B amorphous alloy delivered 1.8 times faster treatment than the

* Corresponding author.
E-mail address: lwy@bjfu.edu.cn (W. Liang).

https://doi.org/10.1016/j.cclet.2024.109492
1001-8417/© 2024 Published by Elsevier B.V. on behalf of Chinese Chemical Society and Institute of Materia Medica, Chinese Academy of Medical Sciences.

Table 1
Properties of common amorphous alloys.

Composition	Main properties	Ref.
Fe-based	High mechanical properties, soft ferromagnetic and high amorphous forming ability	[13]
Cu-based	High Fracture strength and good plasticity	[14]
Mg-based	High corrosion resistance	[15]
Zr-based	High anticorrosion ability in strong acids or alkalis	[16]
Al-based	High wear resistance and corrosion resistance	[17]
Ce-based	Low glass transition temperature and good thermoplasticity	[18]
Co-based	Ultra-high permeability, high hardness and excellent corrosion resistance	[19]
Nd-based	High hard magnetic properties	[20]
Ti-based	Light weight, low density, high specific strength, large compressive strength, reasonable Young's modulus and good corrosion resistance	[21]

crystalline counterpart in treating direct blue 6 [31]. In addition, the catalyst regeneration and recyclability improvement are also important to realize practical applications using the metal-based catalysts [32]. Amorphous alloy ribbons with excellent stability have potential prospects in the field of practical water treatment. At present, there already have been some reviews on the processing method, properties, catalytic performance and applications of amorphous alloys in wastewater treatment [27,29,33]. However, as more and more attentions and developments have been paid to amorphous alloys, the study of their catalytic applications has also increased rapidly. Therefore, it is essential to provide a comprehensive summary of recent achievements in water or wastewater treatment using amorphous alloys as catalysts.

In this paper, the preparation of amorphous alloys, particularly as catalysts, is initially introduced to demonstrate the variety of morphology. Then, the developments in the effects of their physical characteristics, such as atomic components, electronic structure and atomic configuration, on catalytic performance are described. Additionally, the present review shows several benefits of using amorphous alloys in catalytic degradation processes, including experimental parameter effects, stability and reusability in environmental applications. Existing catalytic mechanisms, such as oxidative and reductive degradation, are also discussed in detail. The last section summarizes a few remaining technical challenges, presenting future directions in this field.

2. Amorphous alloys

Amorphous alloys are materials whose atomic structure differs from traditional crystalline alloys [34], which can be determined by characterization (Note S1 and Fig. S1 in Supporting information). The atomic arrangement of amorphous alloys shows the characteristics of short-range order and long-range disorder (Fig. S2a in Supporting information). It implies that the atoms in amorphous alloys are arranged in space without periodicity and translational symmetry. In contrast, the bonding (parameters such as coordination number, atomic spacing, bond angle and bond length) between the nearest or next nearest neighbor atoms has certain regularity [35]. In general, the short-range order can be divided into chemical and geometrical short-range order. The chemical short-range order is used to describe the chaotic state of the various elements in the alloy. It is mainly used to measure the degree that the chemical composition around each atom deviates from the average composition of the entire alloy. The geometrical short-range order describes the structure of the alloy from the geometric arrangement, ignoring the differences in element types and regards each atom as an abstract geometric point. The atomic bonding mode of amorphous alloys is mainly based on metal bonds, which have no directionality. Therefore, it has some characteristics of metals and alloys [36,37]. Currently, the technology for preparing these alloys is well-developed (Note S2 in Supporting information). The amorphous formation is based on the transition between the metastable liquid phase and metastable phase (Fig. S2b in Supporting information). The preparation methods of amorphous alloys are briefly summarized in Table S1 (Supporting information) and the schematic diagrams in Figs. S2c, S3, and S4 (Supporting information).

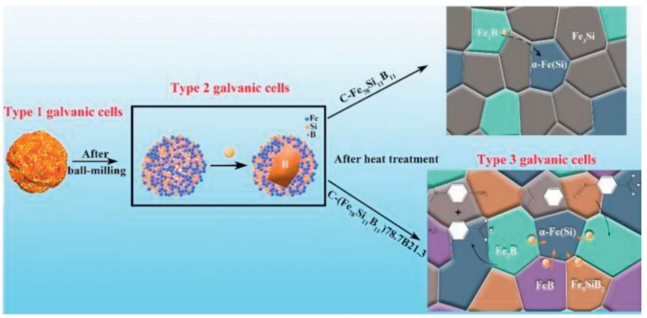

Fig. 1. Schematic illustration of the different degradation mechanisms for B element facilitated Fe-based amorphous alloy catalysts. Reprinted with permission [43]. Copyright 2019, Wiley-VCH Verlag GmbH & Co. KGaA, Weinheim.

2.1. Physical characteristics

Only a few specific elements and alloys have been applied as catalytic materials, although many combinations of elements in the periodic table could form amorphous structures [38]. Generally, there are mainly two types of amorphous alloys used as catalysts. One type is transition metals of VIII group in the periodic table and metalloid combination, such as Fe-B, Ni-B, Ni-P and Co-Si-B. Another type is a metal and metal combination, such as Cu-Zr and Ni-Zr [39]. Easy manipulation of atomic composition is a superior advantage for amorphous alloys in the catalytic field [40]. Adding metal elements could not only improve the stability of these structures but also adjust the electronic structure [41]. Zhang *et al.* compared the effects of Co, Cr and Ni addition on the Fe-Si-B in the degradation of acid orange II [42]. They discovered that Co could reduce the activation energy without losing catalytic efficiency. Simultaneously, Cr eradicated the dye degradation ability across a wide temperature range, and Ni changed the decolorization mechanism from dye degradation to dye adsorption. For the addition of metalloids (Fig. 1), adding B facilitated hybrid structures of Fe-based amorphous alloys [43]. Moreover, the generation of three galvanic cells improved degradation efficiency of methyl orange.

2.2. Electronic structure

It is well known that the electronic structure of a catalyst could play a vital influence on the catalytic performance. Moreover, an electron could be an efficient catalyst to promote different radical cascade reactions [44]. Unlike the crystalline catalysts with a highly ordered atomic structure, the amorphous alloys with a disordered atomic structure could possess plentiful possibilities to tai-

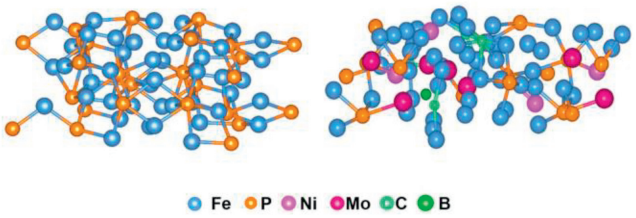

Fig. 2. Atomic configuration of Fe_3P and amorphous alloy components calculated by DFT. Reprinted with permission [47]. Copyright 2021, American Chemical Society.

lor their electronic structures in the catalytic application. Hu *et al.* found that the $Ni_{40}Fe_{40}P_{20}$ possesses the metallic Ni-Ni and Fe-Fe bonds and the Ni-P and Fe-P bonds due to partial Ni or Fe atoms coordinated with P atoms [45]. The formation of Ni-P and Fe-P bonds improved the electron transport at a moderate distance, facilitating the optimization of their electronic structure and thereby promoting the corresponding catalytic efficiency.

2.3. Atomic configuration

Compared with the well-defined atomic configuration in crystalline catalysts, the amorphous alloy catalysts could provide more active sites in catalytic reactivity. Hu *et al.* found that the Pd-based amorphous alloys could possess many active sites with various local atomic packing structures [46]. In addition, the atomic configuration of these Pd-based alloys could also significantly contribute to the catalytic performance of the material. Yang *et al.* prepared the three-dimensional hierarchical porous architectures introducing Cu as a reductant into amorphous alloys *via* laser 3D printing technique [47]. The materials exhibited exceptional catalytic efficiency in degrading Rhodamine B. Due to the crystallization of the amorphous phase during the 3D printing process, a certain proportion of nanocrystalline Fe-based metal phosphides was formed in the catalysts, exhibiting a positive effect on the catalytic activity. The theoretical calculations using density functional theory (DFT) obtained the atomic configuration of Fe_3P and amorphous alloy components (Fig. 2). It was indicated that amorphous alloy and metal phosphides were the main active species in the catalysts for activation of H_2O_2. Such outstanding synergetic atomic configurations are almost unachievable in crystalline catalysts with a specific atomic packing structure, further proving the potential applicability of these alloys in catalysis.

2.4. Relaxation

Following the discovery of the unique atomic packing structures of long-range disorder and short-range order, there have been many studies on the underlying structural evolution of amorphous alloys [48]. In general, relaxation phenomena are normally undesirable in structural applications because they result in brittleness. Recently, Chang *et al.* found that the fast relaxation in amorphous alloys could continue the dynamics of high-temperature liquids [49]. Its carriers could rapidly diffuse, making liquid-like atoms inherited from high-temperature liquids. Molecular dynamics simulations revealed that this fast relaxation arose from string-like diffusion of the liquid-like atoms in these alloys. Importantly, the motions of liquid-like atoms could form string-like structures, suggesting that the fast diffusion of these atoms in amorphous alloys is not random but cooperative. These findings could clarify the mechanism of fast relaxation and reveal deeper insights into the nature of glasses and the glass transition. However, rare work has been done on the effect of relaxation in applied catalysis. Therefore, the effects of the atomic rearrangement during the relaxation on catalysis of amorphous alloy still require more attention.

3. Environmental applications

3.1. Heavy metal ions

Amorphous alloys have been proven to exhibit excellent removal properties for heavy metals in wastewater. Yan *et al.* used $Fe_{78}Si_9B_{13}$ amorphous ribbons to remove copper ions from wastewater by a spontaneous redox reaction and the displacement reaction of copper ions [50]. The report demonstrated that $Fe_{78}Si_9B_{13}$ could help the electrons rapidly transfer from iron atoms in the active atomic layer to copper ions owing to its unique surface mobility. Abundant galvanic cells are produced due to iron and copper, which is beneficial to the reaction process. In contrast, the surface mobility of the crystalline iron ribbons was much weaker than the alloys due to the stable thermodynamic state. Consequently, amorphous alloys showed higher removal efficiency on heavy metals, lower reaction activation energy and higher corrosion current density than crystalline iron. Liang *et al.* employed $Fe_{78}Si_9B_{13}$ amorphous alloys in real industrial contaminated water treatment by investigating effective separation of arsenic and reduction of nitrate [51]. They confirmed Fe-based amorphous alloys demonstrates attractively high removal rate of arsenic in 30 min, which is ascribed to synergistic effect of reduction/adsorption by amorphous alloys, precipitation of arsenic sulfide and adsorption of generated iron sulfide. On the other hand, 20 reused times of Fe-based amorphous alloys for nitrate reduction suggests remarkable sustainability.

3.2. Phenolic compounds

For much industrial wastewater, such as the petrochemical industry, pesticides and insecticides, phenolic compounds pose a great threat to the aquatic system due to their toxicity and poor biodegradability [52]. Amorphous alloys have been proposed for the degradation of phenolic compounds [53]. Wang *et al.* used $Fe_{78}Si_9B_{13}$ as heterogeneous Fenton catalysts in the phenol degradation process [54]. More than 99% of phenol was completely removed within 10 min for a solution containing 1000 mg/L of phenol. They also demonstrated that phenol was degraded by $^{\bullet}OH$ decomposed by H_2O_2 on the surface of $Fe_{78}Si_9B_{13}$. The results suggested that the H_2O_2 was first adsorbed onto the surface of $Fe_{78}Si_9B_{13}$ to produce $^{\bullet}OH$. The $^{\bullet}OH$ reacted with phenol in the *ortho* and *para* positions to form catechol and hydroquinone. Further oxidation of the dihydroxybenzenes occurs to produce benzoquinones, and the phenolic ring opens to form lower molecular weight organic compounds that are ultimately oxidized to CO_2 and H_2O.

3.3. Antibiotics

Wan *et al.* fabricated TiO_2 nanowires decorated with a trace amount of amorphous Fe-Si-B microspheres, forming hybrid films by the simple painting method [55]. They demonstrated excellent photo degradability of antibiotic contaminants by these hybrid films. It was found that the films containing 1 wt% Fe-Si-B exhibited great tetracycline degradation at general pH conditions from 2 to 12. The degradation efficiencies of tetracycline reached 98.2% at pH 2 and 85.5% at pH 12 within 4 h. Moreover, the enhanced reusability was attributed to the corrosion resistance of amorphous microspheres Fe-Si-B wound around the TiO_2 nanowires.

3.4. Oily wastewater

Oily wastewater, usually made up of oil and grease, contains high chemical oxygen demand (COD) due to the presence of multiplicate aromatic hydrocarbons and phenolic compounds. Xu

et al. prepared $Fe_{78}Si_9B_{13}$ amorphous ribbons to treat simulated petroleum wastewater by a Fenton-like process [56]. The COD and oil & grease removal rates could reach up to 79.6% and 84.6%. It is worth mentioning that the amorphous ribbons exhibited good structural stability, presenting an excellent catalytic performance for petroleum wastewater treatment.

3.5. Dyeing wastewater

Numerous reports indicated the degradation of dyeing wastewater or simulated solution using amorphous alloys. The destruction of the chromophore could be considered the main reason for decolorizing dyes [57]. In general, two oxidation processes are considered functional for dyes degradation by amorphous alloys. On the one hand, direct oxidation of dye molecules by electron transfer reaction. Conversely, indirect oxidation generates reactive radicals by activating peroxides [58]. The decomposition of dyes in forming aromatic intermediates is further oxidized to ring opening products and final products of inorganic substances.

3.6. Coking wastewater

Coking wastewater from steel-making industries generally contains phenols, ammonia, cyanides, thiocyanate, polycyclic aromatic compounds, and other contaminants. Its complex composition and high concentration result in heavy chroma and high COD [59]. Qin *et al.* applied two types of coking wastewater before anaerobic treatment and after aerobic treatment to examine the catalytic performance of $Fe_{78}Si_8B_{14}$ in a Fenton-like system [60]. Results showed that $Fe_{78}Si_8B_{14}$ amorphous alloys exhibited a superior catalytic capability and the COD removal efficiency of coking wastewater before anaerobic treatment. After the aerobic treatment, 71% within 30 min and 89% within 60 min were achieved under the optimal condition, respectively.

3.7. Other organic wastewater

The chemical bonds of the organic compounds in complex and high concentrations are usually difficult to break, which leads to the ineffectiveness of traditional oxidation materials. Yang *et al.* investigated the treatment of high-concentration organic wastewater using $Fe_{78}Si_9B_{13}$ amorphous alloys in the Fenton-like system [61]. The high-concentration organics in wastewater mainly consisted of methylbenzene and methanol, with COD being 43,639 mg/L. Results showed that the ultimate removal by amorphous alloys was as high as 85%. It has also been proved that the $Fe_{78}Si_9B_{13}$ played an excellent catalytic activity in the oxidative degradation of organic compounds. Its microstructure transformation during the corrosion process promoted the degradation efficiency of the wastewater treatment process. In fact, industrial wastewater is a coexistence system with many kinds of pollutants. The effect of the interwoven system on the degradation performance needs to be thoroughly considered. Li *et al.* found that the degradation of carbamazepine in their system was not or little affected by the water matrices [62], including organic matter, various inorganic anions (Cl^-, SO_4^{2-}, NO_3^-) and cations (Na^+, K^+, Ca^{2+}, Mg^{2+}) (Fig. S5 in Supporting information). $H_2PO_4^-$ was found to suppress the reaction significantly because it prevented the formation of active species.

4. Catalytic degradation processes using amorphous alloys

4.1. Processes and mechanisms

Several types of wastewater with high organic concentrations have been successfully degraded using amorphous alloy catalysts. Recently, amorphous alloys containing transitional metals were reported as advanced reductive agents owing to efficient chemical reactivity and strong surface stability [31,63]. The reductive chemical reactivity could be strongly based on the electron transfer ability of the catalysts. Due to the disordered atomic packing structure, it would be easier to activate amorphous alloys with weak atomic bonding than to activate their crystalline counterparts. This could provide better electron mobility in the solution to further enhance the organic pollutants' ability to gain electrons [64]. The degradation of pollutants using amorphous alloys also could be combined with AOPs. The catalytic efficiency could be highly dependent on several operational parameters based on the specific processes [65]. In addition, to investigate degradation efficiency, the *pseudo*-first-order kinetic model is often employed (Eq. 1). Table 2 [12,41,42,64,66-79] summarizes the kinetic rate (k_{obs}) of wastewater degradation by various compositions of amorphous alloys.

$$\ln C_0/C_t = k_{obs} \cdot t \quad (1)$$

where C_0 and C_t are wastewater concentrations at the initial time and time t, respectively.

4.1.1. Combined with Fenton-like process

Amorphous alloys were first used to degrade dye wastewater in 2010. It was found that the Fe-Mo-Si-B achieved a 4 times faster degradation rate than the corresponding crystalline alloy in treating direct blue 2B [73]. Zuo *et al.* used $Fe_{80}Si_{10}B_{10}$ and $Fe_{83}Si_5B_8P_4$ ribbons to degrade methyl blue and rhodamine B by Fenton-like oxidation and found that the color removal reached nearly 100% within 11 min for both the dyes [80]. Wang *et al.* revealed that $Fe_{83}Si_5B_8P_4$ enhanced the efficiency of phenol and rhodamine B degradation in combination with H_2O_2 [54]. Zhao *et al.* degraded acid orange II using $Cu_{47.5}Zr_{46}Al_{6.5}$ amorphous ribbons [81]. The catalytic mechanism they proposed can be illustrated in Fig. S6 (Supporting information), which followed two pathways: corrosion reaction and catalytic degradation process. The interaction between H^+ and Cl^- will invade and attack the surface of the ribbons because of the pitting reaction, bringing about the copper nanoparticles to be exposed naturally in solution. The exposed copper nanoparticles and the produced Cu_2O with strong reducing ability can directly reduce the dye molecules in the solution. In addition, they can both destroy O_2 molecules to develop $^{\bullet}OH$ under acidic conditions and oxidize azo dye molecules. Moreover, a mere handful of Al elements also have a certain contribution in the catalytic degradation experiments. The first part can be interpreted as the direct reduction of zero-valent Al. Secondly, new reduced hydrogen [H] can act on the reduction of azo bonds under the action of surface catalysis.

4.1.2. Combined with ultrasonic vibration process

As a kind of physical field, the ultrasonic treatment approach could have satisfactory catalytic oxidation characteristics in the chemical reaction process, which can produce $^{\bullet}OH$ to induce and promote a chain reaction of free radicals and ultimately achieve the purpose of degradation and treatment of organic wastewater [82]. Lv *et al.* found that ultrasonic vibration could achieve an effective approach that could dramatically improve the degradation of methylene blue using industrial $Fe_{78}Si_9B_{13}$ amorphous powders [83]. Fig. S7 (Supporting information) illustrates the pathway of the degradation process. Metallic iron from $Fe_{78}Si_9B_{13}$ amorphous powders reacts with H_2O_2 in the acidic methylene blue solution and generates the strong oxidizing $^{\bullet}OH$. Then, methylene blue molecules undergo redox reaction and are decomposed into small molecules including H_2O and CO_2 by cleavage of interlinkage. The work indicates that the micro-channels on the surface of or inside $Fe_{78}Si_9B_{13}$ particles could offer a shortcut for fast mass transfer and supply plenty of reactive sites with low density and high

Table 2
The k_{obs} of several amorphous alloys in wastewater degradation.

Composition	Morphology	Organic pollutants	k_{obs} (min^{-1})	Ref.
$Fe_{82}B_{18}$	Ribbon	Direct blue 6	0.113	[66]
$Fe_{84}B_{16}$	Ribbon	Direct blue 6	0.110	
$Fe_{78}Si_9B_{13}$	Ribbon	Methylene blue	0.356	[64]
$Fe_{78}Si_9B_{13}$	Ribbon	Malachite green	0.519	
$Fe_{78}Si_9B_{13}$	Ribbon	Methylene blue	0.381	[67]
$Fe_{78}Si_9B_{13}$	Ribbon	Methylene blue	0.640	[68]
$Fe_{78}Si_9B_{13}$	Ribbon	Brilliant red 3B-A	0.668	[69]
$Fe_{78}Si_9B_{13}$	Ribbon	Rhodamine B	0.725	[70]
$Fe_{78}Si_9B_{13}$	Powder	Acid orange II	0.02	
$Fe_{78}Si_8B_{14}$	Ribbon	Acid orange II	0.443	[71]
$Fe_{80}P_{13}C_7$	Ribbon	Methylene blue	0.56	[72]
$Fe_{68}Si_8B_{14}Co_{10}$	Ribbon	Acid orange II	0.317	[42]
$(Fe_{0.99}Mo_{0.01})_{78}Si_9B_{13}$	Ribbon	Direct blue 2B	0.136	[73]
$(Fe_{0.99}Mo_{0.01})_{78}Si_9B_{13}$	Ribbon	Acid orange II	0.282	[74]
$Fe_{77.2}Mo_{0.8}Si_9B_{13}$	Ribbon	Acid orange II	0.282	[75]
$Fe_{76}Si_9B_{10}P_5$	Powder	Direct blue	0.241	[76]
$Fe_{76}Si_9B_{10}P_5$	Powder	Methyl orange	0.151	
$Fe_{83}Si_2B_{11}P_3C_1$	Ribbon	Rhodamine B	0.36	[41]
$Fe_{73.5}Si_{13.5}B_9Cu_1Nb_3$	Ribbon	Methyl orange	0.152	[67]
$Fe_{73.5}Si_{13.5}B_9Cu_1Nb_3$	Ribbon	Methylene blue	0.201	
$Fe_{73.5}Si_{13.5}B_9Cu_1Nb_3$	Ribbon	Malachite green	0.199	[12]
$Fe_{73.5}Si_{13.5}B_9Cu_1Nb_3$	Ribbon	Brilliant red 3B-A	0.184	[69]
$Fe_{73.5}Si_{13.5}B_9Cu_1Nb_3$	Ribbon	Eosin Y	0.876	[77]
$Fe_{73.5}Si_{13.5}B_9Nb_3Cu_1Ni_{8.5}$	Ribbon	Acid orange II	0.16	[78]
$(Fe_{73.5}Si_{13.5}B_9Nb_3Cu_1)_{91.5}Ni_{8.5}$	Powder	Acid orange II	4.5	
$Fe_{81}Cu_1Si_2B_{10}P_6$	Ribbon	Methylene blue	0.58	[79]

energy due to the structural regeneration after ultrasonic vibration. In addition, amorphous structures also undergo a severe plastic deformation during ultrasonic vibration, which results in the large residual stress inside each particle. All of these factors contribute to the highly effective reaction of metallic iron with H_2O_2 that occurs on the surface of the loose-packed high-energy powders.

4.1.3. Combined with electricity process

A strong electron transfer process could mainly characterize an electrochemical degradation. Qin *et al.* compared $Fe_{78}Si_9B_{13}$ ribbons with dimensionally stable anode and metal-like boron-doped diamond electrodes in azo dye degradation and found that the $Fe_{78}Si_9B_{13}$ was superior in saving degradation time and energy consumption and improving degradation efficiency [84]. Deng *et al.* used the $Cu_{55}Zr_{45}$ amorphous ribbons as an electrode to degrade acid orange II dyes and reached 95.6% within 40 min for degradation [85]. The degradation can be divided into the following three ways such as direct electron transfer on the surface of the ribbons, the effect of nano-copper on ribbons surface, and the action of active chlorine (Fig. S8 in Supporting information). The primary way of degrading dye molecules is to produce strongly oxidizing activated radicals by copper nanoparticles and oxidized copper at the ribbon surface under acidic conditions. The process is when Cu^0/Cu^+ loses electrons and converts to Cu^+/Cu^{2+}, and it can react with O_2 and H_2O to generate $^{\bullet}OH$ and $^{\bullet}O_2^-$ under acidic conditions. The report demonstrated that the outstanding properties were derived from the unique atomic structure of amorphous alloys and the application of electrochemical technologies. The as-developed method combining amorphous alloys with electrochemical technology could significantly affect the applicability of this material. In addition, amorphous alloys could also be combined with electro-Fenton process. Compared to the traditional Fenton processes, the electro-Fenton process could present the advantages of reducing H_2O_2 and power consumption, electrode mass loss and electrolysis time [86]. During the electro-Fenton treatment of rhodamine B using $Fe_{83}Si_5B_8P_4$, the in-situ production of H_2O_2 by $2e^-$ reduction of dissolved oxygen at the cathode produced hydroxyl radicals with Fe^{2+} improved the degradation efficiency [80]. Moreover, the Fe^{2+} was regenerated by electroreduction of Fe^{3+} on the surface of the cathode, deserving or even avoiding the production of iron sludge [87]. These results suggest that amorphous alloys combined with electricity process could effectively improve the degradation performance in nearly actual wastewater.

4.1.4. Combined with light process

Amorphous alloys were proven to be very effective catalysts in the photodegradation process for wastewater treatment [12,68]. Jia *et al.* reported that Fe-based amorphous alloys exhibited the as-contained advanced catalytic capability when degrading methyl blue and methyl orange in a photo-Fenton oxidation [67]. The production rate of $^{\bullet}OH$ was 5–10 times faster than other Fe-based catalysts. The as-employed UV–vis light energy during the dye degradation significantly enhanced the activation of the electrons on $4s^2$ orbital of the amorphous Fe atoms. In addition, the light energy was also advantageous to Fe^{3+} to convert back to Fe^{2+} when providing more catalyst dosage. The inclusion of Si and B atoms in the amorphous alloys enhances the surface stability thereby improving the reusability [66]. Zuo *et al.* successfully synthesized a series of Fe-B-C-Ti amorphous ribbons to degrade methylene blue under light irradiation [88]. The Fe-B-C-Ti could be activated under visible light, contributing significantly to methylene blue degradation from acidic to neutral pH values. Complete degradation of methylene blue was achieved within 60 min at pH 5 under simulated solar irradiation (Fig. S9 in Supporting information). They also investigated comparing methylene blue degradation with and without adding H_2O_2. It was found that the appropriate addition of H_2O_2 can effectively improve the photocatalytic degradation rate. At the same time, the $Fe_{75}B_{10}C_{10}Ti_5$ ribbons were able to degrade the methylene blue by 100% within 6 min at pH 3, even without adding H_2O_2. Therefore, the $Fe_{75}B_{10}C_{10}Ti_5$ ribbons were effective in pollutant degradation without any addition of oxidant in the acidic environment, which is an excellent property of this amorphous alloy catalyst.

4.1.5. Mechanism

According to the above processes of wastewater treatment using amorphous alloys, it is accepted that the oxidative degradation

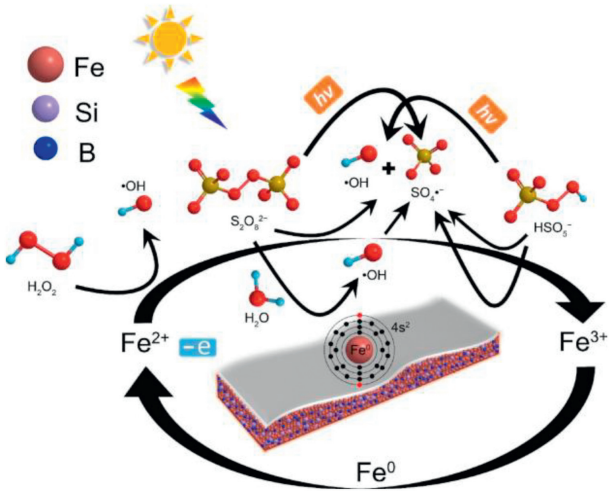

Fig. 3. The generation of radicals from H_2O_2, PS and PMS by amorphous alloys. Reprinted with permission [89]. Copyright 2017, Elsevier B.V.

of pollutants in wastewater is mostly achieved by activating peroxides or persulfate using amorphous alloys to produce reactive radicals, such as $^{\bullet}OH$ and $SO_4^{\bullet-}$. Numerous publications dealt with the reactive species generated by amorphous alloys and their roles in wastewater degradation. Recent reports have demonstrated that amorphous alloys could have an excellent ability to activate peroxides. Liang *et al.* manufactured $Fe_{78}Si_9B_{13}$ amorphous alloy ribbons and compared their activation behavior on three peroxides, namely H_2O_2, PS and PMS [89]. The results showed that $Fe_{78}Si_9B_{13}$ amorphous alloys had an exceptionally high capability for activating these peroxides to produce $^{\bullet}OH$ and/or $SO_4^{\bullet-}$ (Fig. 3). The reactive radicals of H_2O_2 were demonstrated as $^{\bullet}OH$, while the PS and PMS activation mainly generated $SO_4^{\bullet-}$. As shown in Eq. 2, the transitional metals and the generated metal ions could act as electron donors to activate the peroxides using amorphous alloys. Eqs. 3–5 present that during the H_2O_2 activation, the $^{\bullet}OH$ as the main oxidative agent, is finally produced to degrade organics. The as-proposed reactions of PS and PMS by amorphous alloys suggested that both $^{\bullet}OH$ and $SO_4^{\bullet-}$ could be generated from PS (Eqs. 6 and 7) and PMS (Eqs. 8–11). The order of predominant radical generation rate by $Fe_{78}Si_9B_{13}$ activation under UV–vis irradiation was PS > H_2O_2 > PMS.

$$Fe^0 + h\nu \rightarrow Fe^{2+} + 2e^- \quad (2)$$

$$Fe^0 + H_2O_2 \rightarrow Fe^{2+} + 2OH^- \quad (3)$$

$$Fe^{2+} + H_2O_2 \rightarrow Fe^{3+} + OH^- + {}^{\bullet}OH \quad (4)$$

$$^{\bullet}OH + \text{organics} \rightarrow \text{products} \quad (5)$$

$$Fe^0 + 2S_2O_8^{2-} \rightarrow Fe^{2+} + 2SO_4^{\bullet-} + 2SO_4^{2-} \quad (6)$$

$$Fe^{2+} + S_2O_8^{2-} \rightarrow Fe^{3+} + SO_4^{\bullet-} + SO_4^{2-} \quad (7)$$

$$Fe^0 + 2HSO_5^- \rightarrow Fe^{2+} + 2SO_4^{\bullet-} + 2OH^- \quad (8)$$

$$Fe^{2+} + HSO_5^- \rightarrow Fe^{3+} + SO_4^{\bullet-} + OH^- \quad (9)$$

$$SO_4^{\bullet-} + H_2O \leftrightarrow {}^{\bullet}OH + H^+ + SO_4^{2-} \quad (10)$$

$$^{\bullet}OH/SO_4^{\bullet-} + \text{organics} \rightarrow \text{products} \quad (11)$$

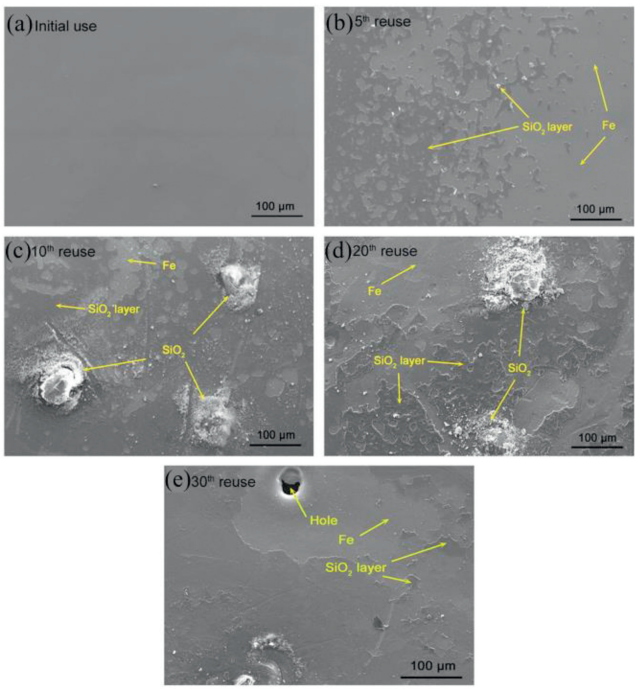

Fig. 4. SEM micrographs of $Fe_{78}Si_9B_{13}$ amorphous alloys of (a) initial use; (b) 5th use; (c) 10th use; (d) 20th use; (e) 30th use. Reprinted with permission [68]. Copyright 2016, The Author(s).

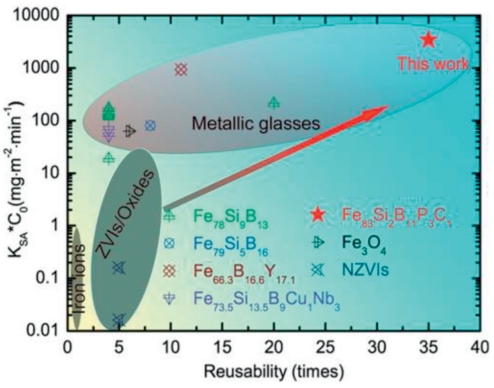

Fig. 5. Comparison of degradation capability *versus* reusability for various amorphous and crystalline catalysts. Reprinted with permission [41]. Copyright 2019, Wiley-VCH Verlag GmbH & Co. KGaA, Weinheim.

4.2. Stability and reusability

Surface stability and catalytic reusability of amorphous alloys have always been important topics in practical applications. It was reported that $Co_{65}Mo_{15}B_{20}$ exhibited excellent reusability in the treatment of blue 6. The degradation efficiency achieved 97% after 20 times of use due to the synergistic coordination of Co and Mo bimetals and the self-exfoliation effect of the corrosion products [90]. Similar results, such as 35 times of $Fe_{83}Si_2B_{11}P_3C_1$ [41] in degradation of rhodamine B, 20 times and 19 times reusability of $Fe_{81}Cu_1Si_2B_{10}P_6$ [79] and $Fe_{80}P_{13}C_7$ [72] in methylene blue degradation, were also achieved. Jia *et al.* developed $Fe_{78}Si_9B_{13}$ alloys that could be reused up to 30 times while maintaining an acceptable methylene blue degradation rate [68]. This was attributed to the production of SiO_2 layer to protect the buried Fe (Fig. 4).

The comparable results of degradation capability *versus* reusability for various ion states, as well as for amorphous and crystalline Fe-based catalysts, are summarized in Fig. 5. The ion-

Table 3
Catalytic advantages compared to the crystalline counterparts.

Amorphous alloys *vs.* commercial iron powder	Organic pollutants	Degradation efficiency	Ref.
$Fe_{80}B_{20}$	Direct blue 6	89 times higher	[66]
$Fe_{76}B_{12}Si_9Y_3$	Methyl orange	1000 times higher	[30]
$Fe_{73}Nb_3Si_7B_{17}$	Azo dye	200 times higher	[31]
$Mg_{73}Zn_{21.5}Ca_{5.5}$	Direct blue 6	1000 times higher	[63]
Amorphous alloys *vs.* crystallized ribbon	Organic pollutants	Degradation efficiency	Ref.
$Fe_{80}B_{20}$	Direct blue 6	1.8 times higher	[90]
$Fe_{78}Si_8B_{14}$	Acid orange II	10 times higher	[71]
$Fe_{78}Si_9B_{13}$	Malachite green	3.5 times higher	[64]
$Fe_{73.5}Si_{13.5}B_9Nb_3Cu_1Ni_{8.5}$	Orange II	Higher reactivity	[78]
$Fe_{77.2}Mo_{0.8}Si_9B_{13}$	Acid orange II	≈3 times higher	[75]

Table 4
Comparison of E_a between amorphous alloys and ordinary crystalline catalysts in wastewater treatment.

Composition (amorphous alloys)	Organic pollutants	E_a (kJ/mol)	Ref.
Fe_xB_{100-x} (x = 80, 82, 84)	Direct blue 6	25.43	[66]
FeBC	Acid orange 7	6.24	[92]
FePC	Acid orange 7	16.59	
$Fe_{78}Si_9B_{13}$	Acid orange II	27.4	
$Fe_{78}Si_9B_{13}$	Rhodamine B	27.9	[70]
$Fe_{78}Si_9B_{13}$	Naphthol green B	20.91	[93]
$Fe_{78}Si_9B_{13}$	Malachite green	43.39	
$Fe_{78}Si_9B_{13}$	Methyl orange	17.63	
$Fe_{68}Si_8B_{14}Co_{10}$	Acid orange II	18.4	[42]
$Fe_{72}Si_2B_{20}Nb_6$	Direct blue 15	34.6	
$(Fe_{0.99}Mo_{0.01})_{78}Si_9B_{13}$	Acid orange II	28.4	[74]
$Fe_{76}B_{12}Si_9Y_3$	Methyl orange	22.6	[30]
$Fe_{76}Si_9B_{10}P_5$	Methyl orange	19.5	[76]
$Fe_{76}Si_9B_{10}P_5$	Direct blue 6	26.8	
$Fe_{83}Si_2B_{11}P_3C_1$	Rhodamine B	29.3	[41]
$Fe_{73.5}Si_{13.5}B_9Cu_1Nb_3$	Eosin Y	22.2	[77]
$Fe_{73.5}Si_{13.5}B_9Cu_1Nb_3$	Methylene blue	49.67	[93]
$Fe_{73.5}Si_{13.5}B_9Cu_1Nb_3$	Naphthol green B	52.36	
$Fe_{73.5}Si_{13.5}B_9Nb_3Cu_1Ni_{8.5}$	Methyl orange	9.8	[78]
$Mg_{73}Zn_{21.5}Ca_{5.5}$	Direct blue 6	51	[63]
Composition (crystalline catalysts)	Organic pollutants	E_a (kJ/mol)	Ref.
Co_3O_4	Phenol	66.2	[94]
Co/SiO_2	Phenol	61.7–75.1	[95]
Co/ZSM-5	Phenol	69.7	[96]
Co/SBA-15	Phenol	67.4–81.4	[97]
Fe_2O_3-ZSM-5	*m*-Cresol	81.3	[98]

state Fe-based catalysts with restricted reusability and the produced Fe sludge secondary pollution have become an impediment to their rapid development. Comparatively, the zero-valence irons and Fe-based oxides with the superiorities of low cost, high efficiency, and large surface area. However, the stability and efficiency of these crystalline catalysts is constrained due to the limitations of their structural defects. The reported reusability of crystalline Fe-based Fenton catalysts is within 10 times. Compared with the ion-state and crystalline alternatives, the recent Fe-based amorphous alloy catalysts present higher essential treating ability and more enhanced stability when degrading organic pollutants. Jia *et al.* reported the $Fe_{83}Si_2B_{11}P_3C_1$ amorphous ribbon belongs to the greatest performance group, with both ultrahigh essential treating ability and a reusability of 35 times without efficiency decay [41].

4.3. Comparison of catalytic properties between the amorphous alloy catalysts and crystalline catalysts

Compared to alloy-based catalysts with a partially crystalline phase, one of the most important properties of amorphous alloys is that the chemical activity could be significantly improved [91]. As it is easier to activate the electrons around the randomly disordered atoms with a weak atomic bonding structure, the high electron mobility in the catalysts will greatly promote the efficiency of wastewater treatment. Table 3 [30,31,63,64,66,71,75,78,90] summarizes the current development of different wastewater using amorphous alloys as catalysts and the advantages compared to the crystalline counterparts or other forms of catalysts, demonstrating the superiorities of using amorphous alloy catalysts in practical applications.

It is worth mentioning that examining the reaction activation energy (E_a) of these alloys in different reaction temperatures could provide important insights into explaining catalytic performance in wastewater treatment. Eq. 12 is the Arrhenius equation employed to demonstrate the E_a for wastewater treatment using amorphous alloys.

$$\ln k = -E_a/RT + \ln A \tag{12}$$

where k is the kinetic rate at different reaction temperatures (T), E_a is the activation energy, R is the gas constant, and A is a constant.

The calculated E_a value could show a significant effect on revealing the potential advantages of amorphous alloy catalysts. Fig. 6 and Table 4 [30,41,42,63,66,70,74,76-78,92-98] summarize the as-calculated E_a values of using amorphous alloys with various atomic components compared to the ordinary crystalline catalysts.

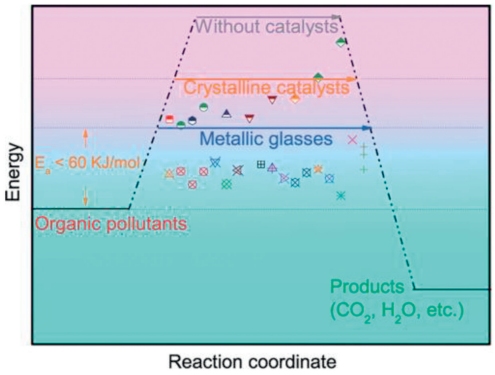

Fig. 6. Comparable results of E_a between the amorphous alloy catalysts and crystalline catalysts. Reprinted with permission [33]. Copyright 2019, Elsevier Ltd.

One of the most important advantages of amorphous alloys is that they present a lower E_a value during wastewater treatment than other catalysts. It was found that the calculated E_a value of using amorphous alloys as catalysts presents a much low value, normally less than 60 kJ/mol, presenting a much lower value than the thermal reactions using ordinary crystalline catalysts (60–250 kJ/mol) [99]. The low value of E_a indicates that less energy is required to pass the reaction barrier, thus making the electrons easier to activate in regard to wastewater treatment.

5. Summary and perspective

The present review has summarized the recent trends in catalytic applications of amorphous alloys as catalysts in wastewater treatment. Amorphous alloys could exhibit several enhancements in oxidative or reductive processes for removing organic pollutants from industrial wastewater. This could be assigned to the unique intrinsic characteristics in contrast with the crystalline catalysts, such as the disordered atomic structure, various compositions, unique electronic structure and atomic configuration. As such, amorphous alloys have tremendous potential in wastewater treatment applications.

The development of novel amorphous alloys with favorable catalytic activity and stability could be an emerging issue. First, the fine-tuning of electronic structure in amorphous alloys could make the atoms randomly coordinate with each other in short range, providing more unsaturated active sites in catalysis. However, a challenge for optimizing further amorphous alloy catalysts is how to improve the electron transfer ability. Second, elemental distribution on amorphous alloys surface could be significant indicator of material stability and reusability. Including specific elements to improve amorphous alloy surface stability was achievable. Therefore, the element introduction and composition regulation of amorphous alloys are important for equilibrium activity and stability. Moreover, the crystallization behavior of amorphous alloys for the wastewater treatment is recently also attractive to investigate their catalytic application. Some methods, such as electrochemical etching, can construct amorphous-nanocrystalline structures and maintain the catalytic activity.

Currently, as a new type of environmental remediation catalyst, the interaction mechanism between amorphous alloys and pollutants is still not clear. It is important to verify the catalytic mechanism of amorphous alloys in different systems and in different pollutant reaction processes. In addition, the application of amorphous alloys in practical water treatment is an important proposition. Due to the special characteristics of amorphous alloys, such as low cost, high surface stability, simple operation process and easy modification of atomic composition, it is reasonable to believe that amorphous alloy catalysts are expected to be valuable in practical application in the future. However, to promote the development of amorphous alloy catalysts, several technical restrictions ranging from the composition's design to reaction optimization of amorphous alloys also need to be overcome.

(1) Reducing the cost and enhancing the reaction efficiency by optimizing the process parameters and improving the catalyst composition with/or surface modification. Moreover, it should focus on establishing the relationship between microstructure and catalytic parameters to reveal the mechanism of performance of these alloys.

(2) Establishing the theoretical relationship between the electronic structure and catalytic performance to improve the electron transport in the moderate distance and provide the possibility for improving the catalytic performance by regulating the electronic structure.

(3) Establishing the relationship between the corrosion failure mechanism and surface atomic structure for improving the sustainability of amorphous alloy catalysts, searching for the new atomic composition of amorphous alloys and constructing a suitable atomic structure for catalytic applications.

(4) The difficulty of composition design of amorphous alloys comes from the uncertainty of amorphous structure. Therefore, adopting the machine learning algorithm to predict the structure and catalytic properties of amorphous alloys and to realize the preparation of amorphous alloys with excellent catalytic properties.

Declaration of competing interest

The authors declare that they have no known competing financial interests or personal relationships that could have appeared to influence the work reported in this paper.

Acknowledgments

The authors are grateful to National Natural Science Foundation of China (No. 51672028), National Water Project of China (No. 2018ZX07105–001) for financial support. We also thank editors and reviewers for their constructive suggestions and comments on this paper.

Supplementary materials

Supplementary material associated with this article can be found, in the online version, at doi:10.1016/j.cclet.2024.109492.

References

[1] F.L. Dong, Z. Pang, S.Y. Yang, et al., ACS Nano 16 (2022) 3449–3475.
[2] Y.W. Fei, N. Han, M.H. Zhang, et al., Chemosphere 307 (2022) 135718.
[3] S. Lim, J.L. Shi, U. von Gunten, D.L. McCurry, Water Res. 213 (2022) 118053.
[4] K.X. Yin, R.X. Wu, Y.N. Shang, et al., Appl. Catal. B: Environ. 329 (2023) 122558.
[5] Z.C. Shangguan, X.Z. Yuan, L.B. Jiang, et al., Chin. Chem. Lett. 33 (2022) 4719–4731.
[6] Y.Y. Zhou, M.C. Cui, Y.M. Ren, et al., Chemosphere 306 (2022) 135547.
[7] K. GracePavithra, P. Senthil Kumar, V. Jaikumar, P. SundarRajan, Rev. Environ. Sci. Biotechnol. 19 (2020) 873–896.
[8] M.X. Yang, Z.X. Hou, X. Zhang, et al., Environ. Sci. Technol. 56 (2022) 11635–11645.
[9] R.D. Su, N. Li, Z. Liu, et al., Environ. Sci. Technol. 57 (2023) 1882–1893.
[10] Y.N. Shang, X.N. Liu, Y.W. Li, et al., Chem. Eng. J. 446 (2022) 137120.
[11] X. Liang, N.H. Fu, S.C. Yao, Z. Li, Y.D. Li, J. Am. Chem. Soc. 144 (2022) 18155–18174.
[12] S. Liang, Z. Jia, W.C. Zhang, W.M. Wang, L.C. Zhang, Mater. Des. 119 (2017) 244–253.
[13] D.S. Song, J.H. Kim, E. Fleury, W.T. Kim, D.H. Kim, J. Alloys Compd. 389 (2005) 159–164.
[14] J.L. Wu, Z. Peng, Appl. Phys. A 124 (2018) 632.
[15] X.L. Zhang, J.L. Sun, J. Luo, B.B. Wang, J.L. Cheng, Mater. Sci. Technol. 33 (2017) 1186–1191.
[16] H.B. Lu, L.C. Zhang, A. Gebert, L. Schultz, J. Alloys Compd. 462 (2008) 60–67.

[17] J. Henao, A. Concustell, I.G. Cano, et al., Mater. Des. 94 (2016) 253–261.
[18] B. Zhang, R.J. Wang, D.Q. Zhao, M.X. Pan, W.H. Wang, Phys. Rev. B 70 (2004) 224208.
[19] J.L. Zhang, Y.M. Wang, C.H. Shek, J. Appl. Phys. 110 (2011) 083919.
[20] L. Xia, M.B. Tang, H. Xu, et al., J. Mater. Res. 19 (2004) 1307–1310.
[21] S.T. Rajan, A.K. Nandakumar, T. Hanawa, B. Subramanian, J. Non Cryst. Solids 461 (2017) 104–112.
[22] W. Klement, R.H. Willens, P.O.L. Duwez, Nature 187 (1960) 869–870.
[23] Y.C. Hu, Y.W. Li, Y. Yang, et al., Proc. Natl. Acad. Sci. U. S. A. 115 (2018) 6375–6380.
[24] D.C. Hofmann, S.N. Roberts, NPJ Microgravity 1 (2015) 15003.
[25] M. Fan, A. Nawano, J. Schroers, M.D. Shattuck, C.S. O'Hern, J. Chem. Phys. 151 (2019) 144506.
[26] S.T. Rajan, A. Arockiarajan, J. Alloys Compd. 876 (2021) 159939.
[27] Q. Halim, N.A.N. Mohamed, M.R.T. Rejab, W.N.W.A. Naim, Q. Ma, Int. J. Adv. Manuf. Technol. 112 (2021) 1231–1258.
[28] S.X. Liang, L.C. Zhang, Mater. Sci. Forum 960 (2019) 200–206.
[29] A. Molnar, Appl. Surf. Sci. 257 (2011) 8151–8164.
[30] S.H. Xie, P. Huang, J.J. Kruzic, X.R. Zeng, H.X. Qian, Sci. Rep. 6 (2016) 21947.
[31] J.Q. Wang, Y.H. Liu, M.W. Chen, et al., Adv. Funct. Mater. 22 (2012) 2567–2570.
[32] Y.N. Shang, Y.J. Kan, X. Xu, Chin. Chem. Lett. 34 (2023) 108278.
[33] L.C. Zhang, Z. Jia, F.C. Lyu, S.X. Liang, J. Lu, Prog. Mater Sci. 105 (2019) 100576.
[34] S.X. Liang, Z. Jia, Y.J. Liu, et al., Adv. Mater. 30 (2018) 1802764.
[35] X.Y. Li, W.Z. Cai, D.S. Li, et al., Nano Res. 16 (2021) 4277–4288.
[36] X. Han, G. Wu, Y.Y. Ge, et al., Adv. Mater. 34 (2022) 2206994.
[37] J.Z. Xie, S. Ewing, J.N. Boyn, et al., Nature 611 (2022) 479–484.
[38] Y. Pei, G.B. Zhou, L. Nguyen, et al., Chem. Soc. Rev. 41 (2012) 8140–8162.
[39] Á. Molnáar, G.V. Smith, M. Bartók, Adv. Catal. 36 (1989) 329–383.
[40] C.J. Byrne, M. Eldrup, Science 321 (2008) 502–503.
[41] Z. Jia, Q. Wang, L.G. Sun, et al., Adv. Funct. Mater. 29 (2019) 1807857.
[42] C.Q. Zhang, Z.W. Zhu, H.F. Zhang, J. Phys. Chem. Solids 110 (2017) 152–160.
[43] S.H. Xie, Y.L. Xie, J.J. Kruzic, et al., ChemCatChem 12 (2020) 750–761.
[44] A. Studer, D.P. Curran, Nat. Chem. 6 (2014) 765–773.
[45] F. Hu, S.L. Zhu, S.M. Chen, et al., Adv. Mater. 29 (2017) 1606570.
[46] Y.C. Hu, Y.Z. Wang, R. Su, et al., Adv. Mater. 28 (2016) 10293–10297.
[47] C. Yang, C. Zhang, Z.J. Chen, et al., ACS Appl. Mater. Interfaces 13 (2021) 7227–7237.
[48] W.H. Wang, J. Appl. Phys. 110 (2011) 053521.
[49] C. Chang, H.P. Zhang, R. Zhao, et al., Nat. Mater. 21 (2022) 1240–1245.
[50] Y.Q. Yan, X. Liang, J. Ma, J. Shen, Intermetallics 124 (2020) 106849.
[51] S.X. Liang, W.C. Zhang, L.N. Zhang, W.M. Wang, L.C. Zhang, Sustain. Mater. Technol. 22 (2019) e00126.
[52] G.F. Lv, D.C. Wu, R.W. Fu, J. Hazard. Mater. 165 (2009) 961–966.
[53] Z. Deng, C. Zhang, L. Liu, Intermetallics 52 (2014) 9–14.
[54] P. Wang, X.F. Bian, Y.X. Li, Chin. Sci. Bull. 57 (2012) 33–40.
[55] L. Wan, C. Li, G. Long, et al., Colloids Surf. A: Physicochem. Eng. Asp. 645 (2022) 128924.
[56] X.C. Xu, Z.L. Shi, K.Q. Qiu, Mater. Res. Express 7 (2020) 045205.
[57] H.Z. Zhao, Y. Sun, L.N. Xu, J.R. Ni, Chemosphere 78 (2010) 46–51.
[58] N.R. Neti, R. Misra, Chem. Eng. J. 184 (2012) 23–32.
[59] P. Pal, R. Kumar, Sep. Purif. Rev. 43 (2014) 89–123.
[60] X.D. Qin, Z.K. Li, Z.W. Zhu, D.W. Fang, H.F. Zhang, J. Phys. Chem. Solids 133 (2019) 85–91.
[61] J.F. Yang, X.F. Bian, Y.W. Bai, X.Q. Lv, P. Wang, J. Non-Cryst. Solids 358 (2012) 2571–2574.
[62] X.Y. Li, R.L. Lv, W.M. Zhang, et al., Water Res. 228 (2023) 119363.
[63] J.Q. Wang, Y.H. Liu, M.W. Chen, et al., Sci. Rep. 2 (2012) 418.
[64] Z. Jia, X.G. Duan, P. Qin, et al., Adv. Funct. Mater. 27 (2017) 1702258.
[65] B.W. Zhao, Y.L. Liu, H. Zhang, et al., Sustain. Mater. Technol. 35 (2023) e00539.
[66] Y. Tang, Y. Shao, N. Chen, K.F. Yao, RSC Adv. 5 (2015) 6215–6221.
[67] Z. Jia, J. Kang, W.C. Zhang, et al., Appl. Catal. B: Environ. 204 (2017) 537–547.
[68] Z. Jia, X.G. Duan, W.C. Zhang, et al., Sci. Rep. 6 (2016) 38520.
[69] Z. Jia, S.X. Liang, W.C. Zhang, et al., J. Taiwan Inst. Chem. Eng. 71 (2017) 128–136.
[70] X.F. Wang, Y. Pan, Z.R. Zhu, J.L. Wu, Chemosphere 117 (2014) 638–643.
[71] C.Q. Zhang, Z.W. Zhu, H.F. Zhang, Z.Q. Hu, J. Environ. Sci. 24 (2012) 1021–1026.
[72] Q.Q. Wang, M.X. Chen, P.H. Lin, et al., J. Mater. Chem. A 6 (2018) 10686–10699.
[73] C.Q. Zhang, H.F. Zhang, M.Q. Lv, Z.Q. Hu, J. Non-Cryst. Solids 356 (2010) 1703–1706.
[74] C.Q. Zhang, Z.W. Zhu, H.F. Zhang, Z.Q. Hu, J. Non-Cryst. Solids 358 (2012) 61–64.
[75] C.Q. Zhang, Q.L. Sun, J. Non Cryst. Solids 470 (2017) 93–98.
[76] N. Weng, F. Wang, F.X. Qin, W.Y. Tang, Z.H. Dan, Materials 10 (2017) 1001.
[77] J.C. Wang, Z. Jia, S.X. Liang, et al., Mater. Des. 140 (2018) 73–84.
[78] S.Q. Chen, G.N. Yang, S.T. Luo, et al., J. Mater. Chem. A 5 (2017) 14230–14240.
[79] Q.Q. Wang, L. Yun, M.X. Chen, et al., ACS Appl. Nano Mater 2 (2019) 214–227.
[80] M.Q. Zuo, S. Yi, J. Choi, J. Environ. Sci. 105 (2021) 116–127.
[81] B.W. Zhao, Z.W. Zhu, X.D. Qin, Z.K. Li, H.F. Zhang, J. Mater. Sci. Technol. 46 (2020) 88–97.
[82] Y.Y. Cai, J.Y. Li, G.F. Qu, et al., Water Environ. Res. 93 (2021) 1243–1253.
[83] Z.W. Lv, Y.Q. Yan, C.C. Yuan, et al., Mater. Des. 194 (2020) 108876.
[84] X.D. Qin, Z.K. Li, Z.W. Zhu, et al., J. Mater. Sci. Technol. 34 (2018) 2290–2296.
[85] Z.W. Deng, B.W. Zhao, S.T. Li, et al., J. Environ. Sci. 136 (2022) 537–546.
[86] K.S. Aneeshkumar, J.S. Tian, J. Shen, Chin. Chem. Lett. 33 (2022) 2327–2344.
[87] V. Poza-Nogueiras, E. Rosales, M. Pazos, M.A. Sanroman, Chemosphere 201 (2018) 399–416.
[88] M.Q. Zuo, M. Moztahida, D.S. Lee, S. Yi, Chemosphere 287 (2022) 132175.
[89] S.X. Liang, Z. Jia, W.C. Zhang, et al., Appl. Catal. B: Environ. 221 (2018) 108–118.
[90] M.F. Tang, L.M. Lai, D.Y. Ding, et al., J. Non-Cryst. Solids 576 (2022) 121282.
[91] Q. Chen, Z.G. Qi, Y. Feng, et al., J. Mol. Liq. 364 (2022) 120058.
[92] F. Miao, Q.Q. Wang, Q.S. Zeng, et al., J. Mater. Sci. Technol. 38 (2020) 107–118.
[93] X.Q. Wang, Q.Y. Zhang, S.X. Liang, et al., Catalysts 10 (2020) 48.
[94] E. Saputra, S. Muhammad, H. Sun, et al., J. Colloid Interface Sci. 407 (2013) 467–473.
[95] P. Shukla, H. Sun, S. Wang, H.M. Ang, M.O. Tadé, Sep. Purif. Technol. 77 (2011) 230–236.
[96] P. Shukla, S. Wang, K. Singh, H.M. Ang, M.O. Tadé, Appl. Catal. B: Environ. 99 (2010) 163–169.
[97] P. Shukla, H. Sun, S. Wang, H.M. Ang, M.O. Tadé, Catal. Today 175 (2011) 380–385.
[98] Y. Yang, H. Zhang, Y. Yan, R. Soc. Open Sci. 5 (2018) 171731.
[99] J.X. Chen, L.Z. Zhu, Catal. Today 126 (2007) 463–470.